FRET from Quantum Dots to Photodecompose Undesired Acceptors and Report the Condensation and Decondensation of Plasmid DNA

Vasudevanpillai Biju,[†,‡,⊥,*] Abdulaziz Anas,[†,¶] Hidetaka Akita,[§] Edakkattuparambil Sidharthan Shibu,[†] Tamitake Itoh,[†] Hideyoshi Harashima,[§] and Mitsuru Ishikawa[†]

[†]Health Research Institute, National Institute of Advanced Industrial Science and Technology (AIST), 2217-14 Hayashi-Cho, Takamatsu, Kagawa 761-0395, Japan, [‡]PRESTO, Japan Science and Technology Agency, Gobancho Building, 7 Gobancho, Chiyoda-Ku, Tokyo 102-0076, Japan, [§]Graduate School of Pharmaceutical Sciences, Hokkaido University, Hokkaido 060-0812, Japan, and [⊥]Also at Faculty of Engineering, The University of Tokushima, 2-1 minamijyousanjima-Cho, Tokushima 770-8506, Japan. [¶]Present address: National Institute of Oceanography, Regional Center, Kochi, India.

ABSTRACT Protection of genes against enzymatic degradation and overcoming of cellular barriers are critical for efficient gene delivery. The effectiveness of gene delivery by nonviral vectors depends mostly on the extent of DNA packaging or condensation. We show that Förster resonance energy transfer (FRET)-mediated photodecomposition of undesired acceptors in doubly labeled plasmid DNA (pDNA) and FRET recovery after acceptor photodecomposition (FRET-RAP) are effective methods for the detection of DNA condensation and decondensation. Our hypothesis is that undesired acceptors within the Förster distance of highly-photostable donors in precondensed DNA can be selectively photodecomposed by FRET. We investigate this hypothesis by the random labeling of pcDNA3.1-GL3 and pUC18DNA with quantum dots (QDs) as the energy donor and AlexaFluor594 or Cy5 as the acceptor. At first, the random labeling generates efficient FRET, also called intrinsic FRET, in precondensed DNA, which prevents us from decoding any changes in the FRET efficiency during DNA condensation. Next, we suppressed the intrinsic FRET by the FRET-mediated photodecomposition of acceptors within the Förster distance of QDs. Conversely, many acceptors kept intact beyond the Förster distance provide us with high FRET efficiency during the condensation of pDNA using protamine. Further, the FRET efficiency is significantly decreased during the decondensation of DNA using heparan sulfate and glutathione. The random labeling of DNA using excess acceptors around photostable donors followed by the FRET-mediated photodecomposition of undesired acceptors can be a promising method for not only the sensitive detection of DNA condensation by FRET but also the customization of biomolecular sensors.

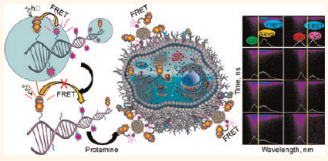

KEYWORDS: FRET · quantum dots · DNA condensation · gene delivery · donor–acceptor

Gene therapy means proper delivery of engineered genetic materials into a host cell and the transcriptional regulation of disease progression.[1] Due to the significant impact of gene therapy in vaccination against specific pathogens and attenuation of genetic disorders, gene delivery has been the subject of extensive investigation over the past two decades.[2–7] Although viral vectors such as retroviruses and adenoviruses are widely applied in gene delivery, viral infection and insertional mutagenesis of the host cells are challenges in the modern gene therapy.[8–12] Additionally, poor transfection of double stranded DNA and nonspecific gene delivery by viral vectors are drawbacks in the targeted and high-speed gene therapy.[12] Because of these drawbacks, encoding of specific genes into plasmid DNA (pDNA) and gene delivery using nonviral vectors are of considerable current interest for the development of vaccines against HIV,[13,14] Influenza A virus subtype H1N1,[15,16] Dengue virus,[17] human papiloma virus,[18] hepatitis virus,[19] *etc.* Nevertheless, the advantages of nonviral systems are counterbalanced by the low efficiency of gene delivery relative to the viral systems. Direct cellular uptake of DNA through the negatively charged cell membrane is hindered by the large size and the negative charge of DNA, suggesting that the condensation and charge-neutralization of DNA are the major prerequisites of efficient gene delivery.[10,20] The condensation of DNA is also a versatile approach for protecting engineered genetic materials against enzymatic degradation *in vivo*.[10]

The condensation of DNA is initiated by the neutralization of its negative charge through electrostatic interactions between its phosphate backbone and an appropriately designed condensing agent such as nanoparticles,[21–23] nanotubes,[24–26] polycations,[27–29] detergents,[30,31] cationic peptides,[32,33] proteins,[20,34] cationic lipids,[35–37]

* Address correspondence to v.biju@aist.go.jp.

Received for review December 12, 2011 and accepted April 2, 2012.

Published online April 02, 2012
10.1021/nn2048608

or by the macromolecular crowding offered by passive polymers.[21,38−40] Subsequently, the complex between DNA and the condensing agent compacts into ordered nanoparticles. The size of such nanoparticles varies significantly (~50 to 200 nm diameter) depending up on the charge and the molecular weight of the condensing agent as well as the size of DNA. Once delivered in cells, the DNA nanoparticles properly decondense, thereby making the engineered genetic material available to bring about the desired changes through transcription and translation. Various techniques such as fluorescence microscopy and spectroscopy,[41−43] electron microscopy,[44−47] dynamic light scattering,[48,49] atomic force microscopy[50−52] and circular dichromism,[53−55] are extensively exploited for validating the efficiency and the extent of DNA condensation. In particular, Förster resonance energy transfer (FRET) between energy donor and acceptor dyes labeled either both at distant locations on a DNA molecule or one on DNA and the other on the condensing agent offers sensitive changes in the FRET efficiency during the condensation and decondensation steps.[56−61] FRET has also been extensively utilized as a premier tool for the distance-dependent molecular sensing using DNA templates and hairpins.[62−67] One of the main advantages of FRET in the evaluation of the condensation of DNA is its sensitivity to report nanometer-scale distance-changes in real-time.[68,69]

The condensation and decondensation of DNA can be efficiently detected by intermolecular or intramolecular FRET. In the former case, DNA molecules are labeled with either acceptors or donors and the condensing agent with the counterpart.[58,70,71] For example; Wang and co-workers[70] have recently shown the usefulness of intermolecular two-step FRET, from quantum dots (QDs) on DNA to first a nucleic acid labeling dye and then Cy5 dye on the condensing agent, for the detection of DNA condensation. One of the advantages of this method is its sensitivity for reporting the coupling between DNA and the condensing agent, but it cannot precisely predict whether the complex between DNA and the condensing agent then compacts into nanoparticles. In the latter case, both the donor and the acceptor are labeled on DNA.[72−77] For example, Turberfield and co-workers have recently shown that the stability of a DNA cage delivered in living cells can be efficiently followed by monitoring the temporal changes in the recovery of the donor's fluorescence during the FRET-mediated photobleaching of acceptors.[72] In another report, Clapp and co-workers have shown that water-soluble Cysteine-coated CdSe/ZnS QDs are capable of sensing the dissociation of DNA/polymer polyplexes.[75] The main advantage of these methods is that donors and acceptors labeled beyond the Förster distance in a DNA molecule precisely report the changes in the intramolecular conformation, the degree of condensation, and the stability of the condensed DNA.[72−77] However, the labeling of DNA with a definite number of donors and acceptors at desired locations is laborious, in particular, without any FRET before the condensation of DNA. We hypothesize that the condensation and decondensation of DNA can be sensitively detected by intramolecular FRET if DNA molecules are randomly labeled with a definite number of donors and excess acceptors followed by the FRET-mediated photodecomposition of undesired acceptors in the precondensed DNA. We investigate this hypothesis by the labeling of

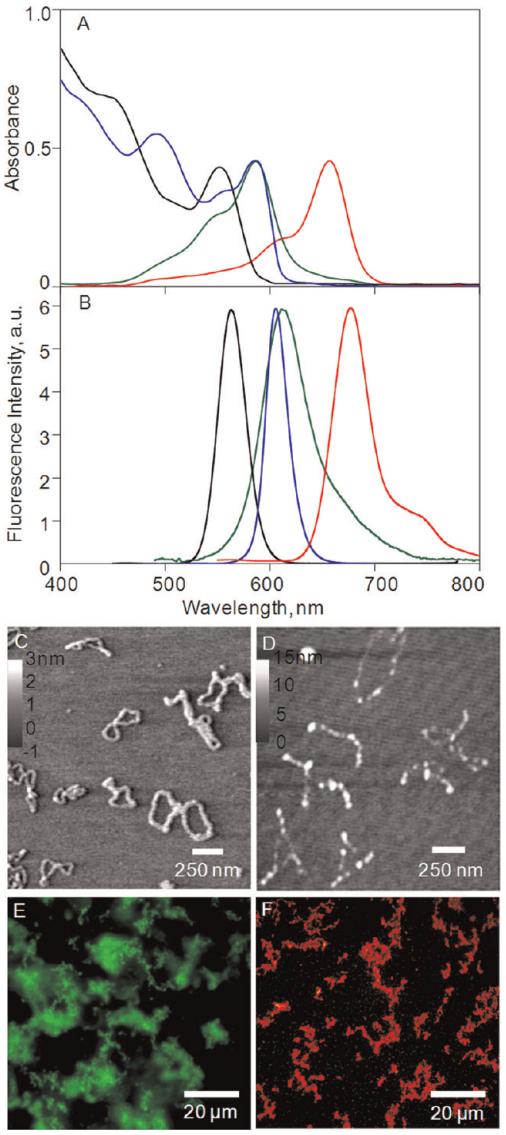

Figure 1. Choosing FRET pairs for the labeling of pcDNA3.1-GL3, pUC18DNA, and the forward and reverse primers of pcDNA3.1-GL3. (A) Absorption and (B) normalized fluorescence spectra of energy donors [QD565 (black traces) and QD605 (blue traces)] and acceptors [AlexaFluor594 (green traces) and Cy5 (red traces)]. (C,D) AFM images of DNA samples: (C) unlabeled pcDNA3.1-GL3 and (D) pcDNA3.1-GL3 labeled using the QD605-Cy5 FRET pair. The poor contrast of pDNA in panel D is due to the saturation of signals from QDs. (E,F) Fluorescence images of pcDNA3.1-GL3 labeled with QD565−AlexaFluor594 FRET pair: (E) image acquired though a band-pass filter for QD565 and (F) image acquired through a 600 nm long-pass filter. The blunt green fluorescence in panel E is due to the scattered excitation light (532 nm).

pDNA (pcDNA3.1GL3 and pUC18DNA) with *ca.* 15 CdSe/ZnS QDs [QD565 (Emλ_{max} *ca.* 565 nm) or QD605 (Emλ_{max} *ca.* 605 nm)] as the energy donor and a large number (*ca.* 150) of AlexaFluor594 or Cy5 as the energy acceptor. The advantages of QDs to be ideal biolabels and energy donors are summarized elsewhere.[78−82] Although strong intrinsic FRET was detected in the precondensed state of the as-labeled DNA, we successfully suppressed it by the selective FRET-mediated photodecomposition of acceptors proximal to QDs. The main advantage of this approach is that even after the photodecomposition of the proximal acceptors, the maximum number of acceptors can be retained beyond the Förster distance for the efficient detection of the condensation−decondensation processes by FRET−RAP.

RESULTS AND DISCUSSION

To identify candidate FRET pairs for the labeling of primers and pDNA molecules and studying the kinetics of the condensation and decondensation of DNA, we recorded the absorption and fluorescence spectra and analyzed the photostability of fluorophores such as Cy3, Cy5, AlexaFluor594, rhodamine B, Texas red, QD565, and QD605. Among these fluorophores, ideal FRET pairs on the basis of their spectral overlap integral are Cy3−Cy5, Cy3−AlexaFluor594, AlexaFluor594−Cy5, QD565−AlexaFluor594, rhodamine B−AlexaFluor594, QD565−Texas red, Cy3−Texas red, Texas red−Cy5, and QD605−Cy5. We selected QD565−AlexaFluor594 and QD605−Cy5 FRET pairs and used them for the labeling of pcDNA3.1-GL3, pUC18DNA, and the forward and reverse primers of pcDNA3.1-GL3. The selected FRET pairs are well comprised for the photostability of donors, FRET-mediated photobleaching of acceptors, overlap between acceptor's absorption and donor's emission spectra (Figure 1A,B), and the Stokes shift.

We next followed three strategies for the labeling of pcDNA3.1-GL3 and pUC18DNA, each with the chosen FRET pairs (QD565−AlexaFluor594 and QD605−Cy5). In the first strategy (Figure 2A, right part), pDNA was first biotinylated using a Mirus Label IT-CX-biotin nucleic acid labeling kit and then labeled with AlexaFluor594 followed by QD565. Here, a platinum complex of AlexaFluor594 is attached to the N7 position of guanine nucleotides. The number of biotin units per DNA is set at *ca.* 15 and the number of AlexaFluor594 per pDNA is set at *ca.* 150. Successively, the sample was treated with the QD565−streptavidin conjugate at 1:15 ratio so that *ca.* 15 QDs are attached to the biotinylated pDNA. In the second strategy (Figure 2A, central part), *ca.* 150 biotin moieties were introduced in pDNA by treatment with a Mirus Label IT-CX-biotin nucleic acid labeling agent. The biotinylated pDNA samples were treated with first Cy5−streptavidin conjugate at 1:150 ratio and then QD605−streptavidin conjugate at 1:15 ratio. The number of dye molecules per pDNA is estimated from the concentrations of the labeling solutions, and the number of QDs per pDNA is estimated using AFM (Figure 1C,D). To further confirm the presence of donors and acceptors on pDNA, we have recorded the fluorescence images of the labeled pDNA samples (Figure 1E,F). Nevertheless, introduction of a large number of QDs (>50) or AlexaFluor594 (>300) in pDNA resulted in the aggregation of DNA (Figure S1, Supporting Information), which is a disadvantage during the condensation and decondensation of DNA. Thus, we limited the number of AlexaFluor594 per DNA to 150 and the number of QDs to 15. In the third strategy (Figure 2A, left part), only one donor and one acceptor were tethered to pcDNA3.1-GL3 by the annealing of Cy5-labeled forward primer (5′-TTGCGCTGCTTCGCGATGTACGGGC-3′) and QD605-labeled reverse primer (5′- TAGAATGACACC-TACTCAGACAATG-3′) at the upstream and downstream regions of the luciferase GL3 insert. Labeling of the primers is shown in Figure 2B. Details about the labeling and purification of pDNA and the primers are provided in the Materials and Methods section.

To validate the importance of labeling of pDNA with excess acceptors and subsequent FRET-mediated photodecomposition of undesired acceptors in the proximity of the donors, we investigated FRET in pcDNA3.1-GL3 after its position-sensitive labeling with one donor and one acceptor (Figure 3A). As discussed above, we incorporated one donor and one acceptor in pcDNA3.1-GL3 by the annealing of single Cy5-labeled forward primer and single QD605-labeled reverse primer at the multiple cloning sites of the DNA. These two regions are spatially separated across 971bp. In other words, the through-bond distance between QD605 and Cy5 in the primer labeled pcDNA should be *ca.* 330 nm, far beyond the calculated Förster distance of 6.07 nm for the QD605−Cy5 pair (details are given later in this section). Thus, the position sensitive labeling of pcDNA3.1 is unlikely to incur any intrinsic FRET in the native state of DNA. As expected, FRET was absent in the precondensed state of the primer bound pcDNA3.1 (Figure 3B). However, there was little FRET even after the condensation of the DNA using protamine (Figure 3C), indicating that QD605 and Cy5 remain beyond the Förster distance in the condensed pcDNA. Alternatively, only one donor and one acceptor do not produce sufficient FRET to be detected after the condensation of DNA because of the low probability for the donor and acceptor to encounter within the Förster distance. Thus, we propose that labeling of pDNA with excess acceptors and subsequent FRET-mediated photodecomposition of undesired acceptors in the proximity of highly photostable donors such as QDs can be a promising strategy for the FRET-based detection of the condensation and decondensation of DNA. This strategy can be promising for hassle-free positioning of donors and acceptors in FRET-based biosensors as well.

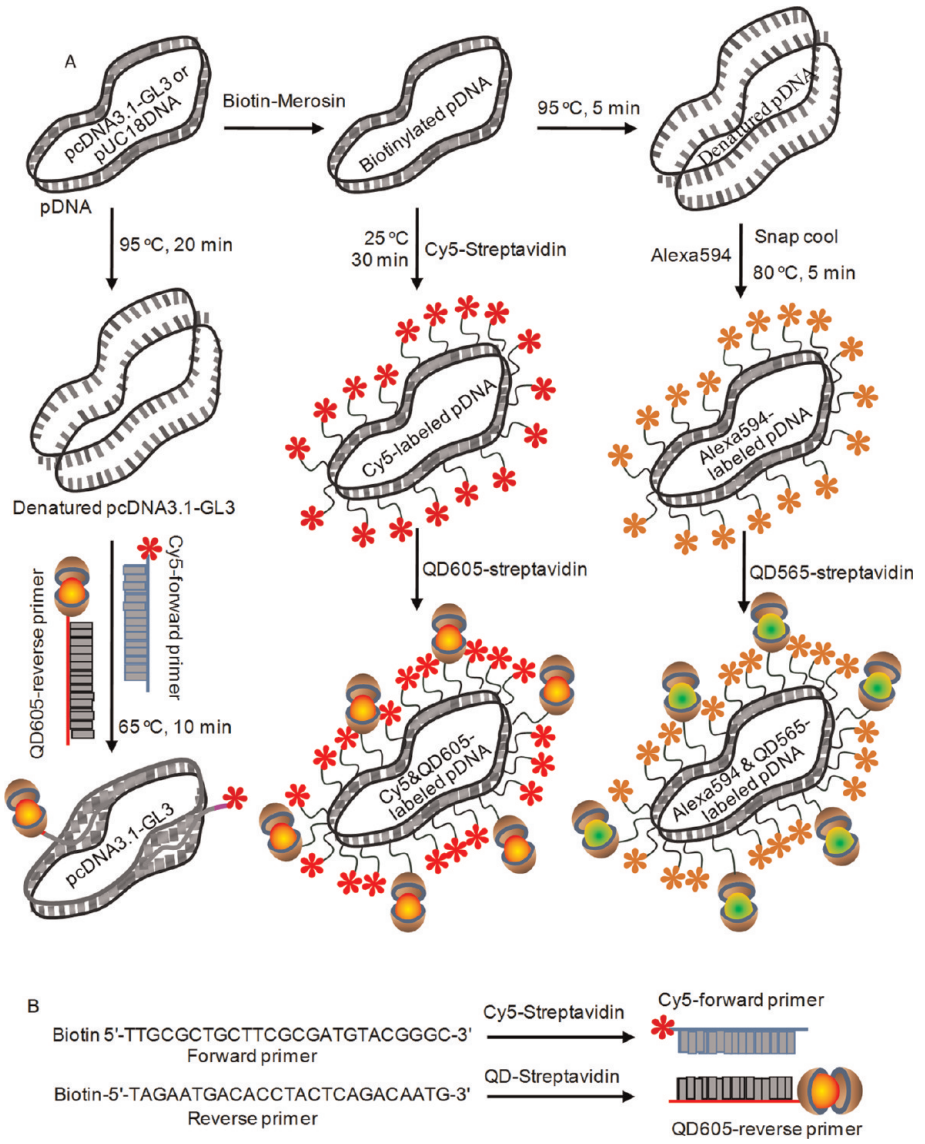

Figure 2. Tagging of plasmids by multiple modes. (A) Labeling of pDNA with energy donors and acceptors: (left) hybridization of Cy5-labeled forward primer (5′-TTGCGCTGCTTCGCGATGTACGGGC-3′) and QD605-labeled reverse primer (5′-TAGAATGACACCTACTCAGACAATG-3′) with pcDNA3.1-GL3; (center) labeling of pcDNA3.1-GL3/pUC18DNA with Cy5 and QD605; and (right) labeling of pcDNA3.1-GL3/pUC18DNA with AlexaFluor594 and QD565. (B) Labeling of the forward primer with Cy5 and the reverse primer with QD605.

To evaluate FRET from QD565 to AlexaFluor594 and from QD605 to Cy5 in the doubly labeled pDNA samples, we recorded and analyzed the fluorescence decays and spectra of the labeled samples. At first, we detected low fluorescence intensities of the donors and exceptionally high FRET efficiency (*ca.* 67%), also called intrinsic FRET, in the as-prepared samples (Figure 4A,E) in which pDNA molecules exist in the native or precondensed state. Details about the calculation of FRET efficiency are provided in the Materials and Methods section. The average fluorescence lifetime of pristine QD605 is 6.85 ns, and this value was lowered to 2.26 ns due to the intrinsic FRET in the as-labeled pDNA samples. The average lifetime values are estimated as $\tau_{av} = (\tau_1\alpha_1 + \tau_2\alpha_2 + \tau_3\alpha_3)/(\alpha_1 + \alpha_2 + \alpha_3)$; where, τ_1, τ_2, and τ_3 are the individual lifetime values, and α_1, α_2, and α_3 are the corresponding amplitudes. The high FRET efficiencies from QD565 to AlexaFluor594 and QD605 to Cy5 are due to the presence of excess (*ca.* 10 times) acceptors in the proximity of each donor. In other words, multiple acceptors are present within the Förster distance of individual QDs even without the condensation of DNA. Thus, by the labeling of pDNA with excess acceptors, we successfully placed a sufficient number of acceptors within the proximity of each donor. However, there was little change in the FRET efficiency even after the condensation of pDNA using protamine because the FRET efficiency was already high in the precondensed DNA. Evaluation of the donor-to-acceptor distance before and after the condensation of DNA is discussed later in this section by following the

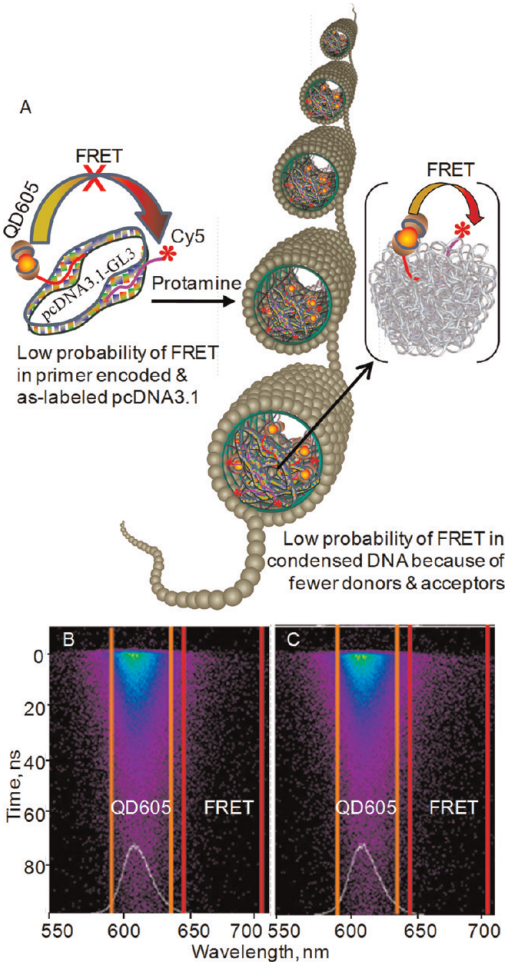

Figure 3. (A) Scheme of the condensation of QD605- and Cy5-labeled-primer-inserted pcDNA3.1-GL3. (B,C) Nanosecond fluorescence decay profiles and fluorescence spectra of a solution of the labeled pcDNA3.1 (25 μg/mL) recorded (B) before and (C) after treatment with protamine (3 mg/mL).

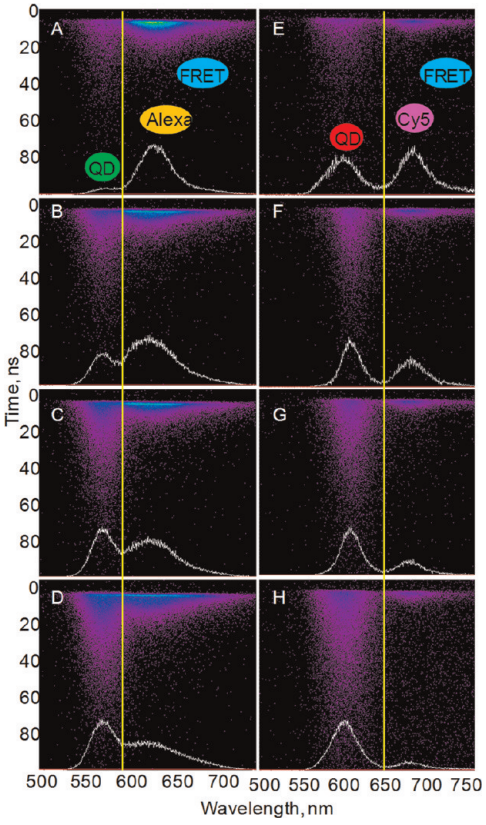

Figure 4. Nanosecond fluorescence decay profiles and fluorescence spectra of pcDNA3.1-GL3 labeled with (A–D) *ca.* 15 QD565–*ca.* 150 AlexaFluor594 FRET pair, and (E–H) *ca.* 15 QD605–*ca.* 150 Cy5 FRET pair. QDs are selectively excited using 400 nm 150 fs laser pulses (6.3 W/cm^2 for panels A–D, and 1.3 W/cm^2 for panels E–H), and the fluorescence decays and spectra were recorded after excitation for (A,E) 0 s, (B,F) 60 s, (C,G) 120 s, and (D,H) 180 s. The fluorescence lifetimes and intensities of QDs are considerably increased during time under excitation due to the FRET-mediated photobleaching of proximal acceptors. Fluorescence decay curves and temporal changes in the fluorescence intensities of the donors and acceptors are provided in the Supporting Information (Figures S2 and S3).

methods discussed by Van Orden and co-workers,[83] Mattoussi and co-workers,[84,85] Wang and co-workers,[86] and Farokhzad and co-workers.[87]

We next employed FRET as an efficient tool for the selective deletion of energy acceptors within the Förster distance of QDs so that the condensation of DNA can be sensitively detected by FRET to AlexaFluor594 or Cy5 molecules retained beyond the Förster distance. Our hypothesis (Figure 5A) is that the condensation and decondensation of pDNA can be sensitively detected by FRET if DNA molecules are randomly labeled with highly photostable but a small number of donors and excess but photolabile acceptors. The key to evaluate this hypothesis is that acceptors within the Förster distance of donors in the precondensed state of DNA can be selectively photodecomposed by FRET-mediated photobleaching. We have investigated this hypothesis by the selective photoactivation of QDs using 400 nm fs pulses (average power = 6.3 W/cm^2 for QD565–AlexaFluor594 system and = 1.3 W/cm^2 for QD605–Cy5 system). As a result, the strong intrinsic FRET from QD565 to AlexaFluor594 (Figure 4A–D) or QD605 to Cy5 (Figure 4E–H) in the as-labeled pDNA molecules is considerably suppressed. As the intrinsic FRET is suppressed, the fluorescence intensity and lifetime of QDs are increased. The temporal changes in the fluorescence decay profiles and fluorescence intensities of the donors and acceptors in the doubly labeled pcDNA3.1-GL3 in its native state and under continuous photoactivation at 400 nm are provided in the Supporting Information (Figures S2 and S3). The suppression of FRET and increase in both the fluorescence intensity and lifetime of QDs suggest that acceptors within the Förster distance of QDs in the precondensed DNA are selectively photodecomposed. In other words, we successfully suppressed the intrinsic FRET due to excess acceptors labeled in the proximity of QDs; whereas, most acceptors beyond the Förster distance remained unaffected. On the other hand, the

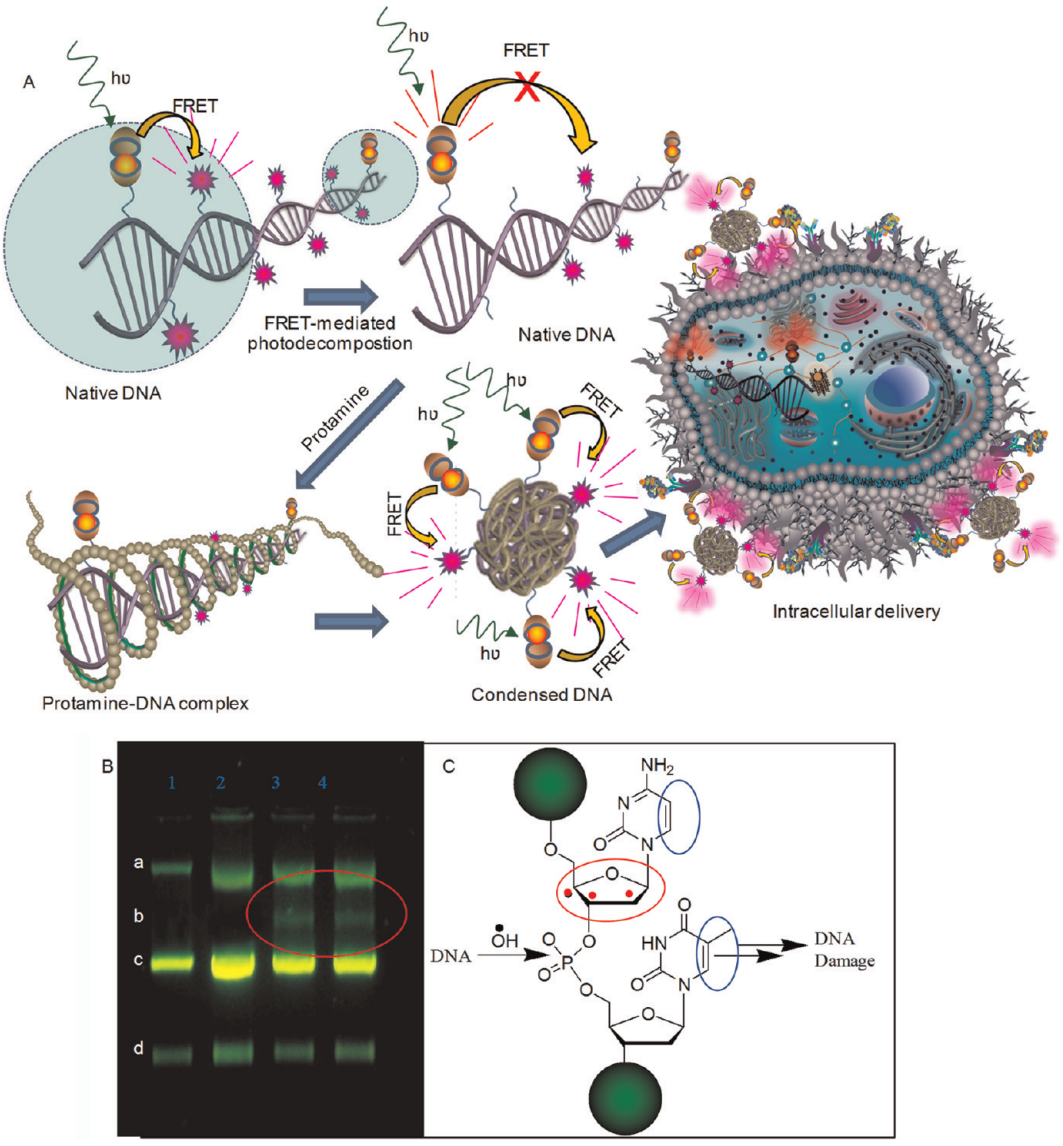

Figure 5. (A) Hypothesis about FRET-mediated photodecomposition of undesired acceptors followed by the sensitive-detection of the condensed DNA in a solution and decondensed DNA in a cell. The large number of acceptors left unaffected beyond the Förster distance can sensitively report the condensation of DNA by FRET-RAP. (B) Agarose gel electrophoresis image of labeled or unlabeled pcDNA3.1-GL3 after photoactivation using 400 nm 150 fs pulses (average power =6.3 W/cm^2): (lane 1) unlabeled DNA illuminated for 60 min, (lane 2) DNA labeled with QD605 but without illumination, (lane 3) DNA labeled with QD605 and illuminated for 30 min, and (lane 4) DNA labeled with QD605 and illuminated for 60 min. (C) Possible pathways of the damage and breakage of QD-labeled DNA under photoactivation. The fluorescent bands in B represent (a) linear, (b) nicked, (c) supercoiled, and (d) circular forms of cybergreen dye-labeled pDNA. The red-circle in B represents DNA damage as a result of prolonged photoactivation of the QD-labeled pDNA. The red and blue circles in C represent the locations of DNA damage identified using base-excision repair enzymes.

fluorescence lifetimes and intensities of free QDs are not considerably affected (Figure S4, Supporting Information) even after 30 min under the above conditions of FRET-mediated photodecomposition of excess acceptors. Between the two acceptors, AlexaFluor594 is more resistant to FRET-mediated photobleaching. Thus, prolonged photoactivation was necessary for the photodecomposition of AlexaFluor594 and the suppression of intrinsic FRET (Figure 4A–D). However, we detected some degree of DNA damage when the QD-labeled pDNA samples are photoactivated for an extended period of time (Figure 5B,C). The damage of DNA under prolonged photoactivation of QDs can be due to the rearrangements and reactions of radical centers produced in the nucleobases or sugar by reactive oxygen intermediates (ROI). These possibilities are considered on the basis of assays involving base excision repair enzymes.[88] Additionally, pDNA molecules labeled with a large number of QDs (>50) or AlexaFluor594 (>250) show aggregation (Figure S1, Supporting Information), which prevented us from obtaining any FRET-RAP after the condensation of DNA. Because of these limitations, we focused our work much on the QD605–Cy5 FRET pair system.

To evaluate the condensation and decondensation of DNA, we applied protamine to the pDNA samples. First, we applied protamine (3 mg/mL) to the pDNA samples in which Cy5 molecules proximal to QD605 were photodecomposed as discussed in the previous paragraph. Then, the condensation process was evaluated by measuring the changes in the fluorescence intensities of both QD605 and Cy5 and the fluorescence lifetime of QD605. Interestingly, as protamine was added to the pDNA samples, submicrometer spheroid fluorescent particles (Figure 6A–C) are formed in the solution. Immediately after the addition of protamine, we detected small fluorescence spots (Figure 6A), which gradually changed into a fluorescent network (Figure 6B) of protamine–pDNA complex and subsequently into larger spheroid particles, resembling the formation of condensed protamine–DNA torroid structures. More importantly, the formation of the fluorescent particles was accompanied by strong FRET emission from Cy5 (Figure 6D,F) and considerable decrease in the fluorescence lifetime (from 6.85 to 2.42 ns) of QDs (Figure 6E,G); that is, the FRET efficiency is estimated at *ca.* 65%. These changes in the fluorescence properties of QDs and Cy5 in pDNA suggest that the fluorescent particles in Figure 6A–C should be condensed complexes between protamine and pDNA. Also, the large FRET values are indicative of efficient condensation of pDNA by protamine.

The condensation of DNA by protamine is a nucleation–growth phenomenon.[1] Protamine, a small arginine-rich nuclear protein that is essential for the dense packaging of DNA during spermatogenesis, electrostatically interacts with the negatively charged DNA, neutralizes the charge of DNA, and condenses *ca.* 50 kb segments of DNA into torroid subunits (Figure 6C). The torroid structure is produced by establishing inter- and intraprotamine disulfide bonds. The first step in the DNA condensation is the spontaneous appearance of nucleation loops (Figure 6B), where the positively charged arginine moieties in protamine interact with the negatively charged phosphate backbone of DNA. This electrostatic interaction results in the neutralization of the charge of DNA and intramolecular collapse of the DNA polymer structure into the proto-torroid structure which gradually grows larger in solution by collecting additional DNA molecules. In addition to the ability of protamine to condense DNA, it maintains DNA molecules unaltered in the condensed state for an extended period of time. Thus, protamine is widely utilized in artificial gene delivery.[1,45–47] Previous approaches for understanding the condensation of DNA by protamine were to obtain AFM images of the condensed DNA on a mica surface[50–52] or colocalized fluorescence images of two fluorescent markers,[41–43] one attached to DNA and the other to protamine, within the diffraction limited area in the condensed DNA. These two approaches are far from reality because the condensation and decondensation of DNA in living systems take place under physiological conditions and within molecular distances. Therefore, knowing how efficiently protamine condenses pDNA in the aqueous phase would be valuable for advancing gene delivery methods. By analyzing changes in the intramolecular FRET, which transpire at molecular distances, we show that the condensation and decondensation of pDNA can be sensitively detected in solution by the FRET–RAP method.

We next tested the decondensation of the pcDNA–protamine complex using either Trisma base or a mixture of heparan sulfate and glutathione. Here, we selected Trisma base and heparan sulfate due to their ability to neutralize the positive charge of protamine. On the other hand, glutathione reduces the intramolecular disulfide bonds in protamine and thus, decondenses DNA by the degradation of the torroid structure. The trace d in Figure 6 panels D,F and E,G shows the fluorescence spectra and decay profiles of QD605- and Cy5-labeled pcDNA3.1-GL3 after condensation using protamine. The traces a, b, and c in Figure 6D–G show the fluorescence spectra and nanosecond fluorescence decay profiles of pristine QD605, as-labeled pDNA, and pDNA after the FRET-mediated photodecomposition of excess Cy5, respectively. As soon as an aqueous solution of Trisma base (3 mg/mL) was added to the condensed DNA sample, we observed a decrease in the fluorescence intensity of Cy5 (Figure 6D, trace e) and a concomitant increase in the fluorescence lifetime of QD605 (Figure 6E, trace e). Here, the FRET efficiency is decreased from *ca.* 61% for the condensed samples to 40% for the sample treated with Trisma base. These observations suggest that Trisma base cannot completely decondense the pDNA that was condensed by protamine. Thus, we replaced Trisma base with a mixture (1:1) of heparan sulfate and glutathione (3 mg/mL). The panels F and G in Figure 6 show the fluorescence spectra and decay profiles of the condensed pcDNA3.1-GL3 before (trace d) and after (trace e) the addition of the heparan sulfate/glutathione mixture, indicating a prominent (from *ca.* 60% to *ca.* 5%) decrease in the FRET efficiency. In other words, a mixture of heparan sulfate and glutathione efficiently decondenses pDNA that was condensed by protamine. On the other hand, the fluorescence intensity and lifetime of QD605 or QD605-only-labeled pDNA sample (Figure S5 and S6, Supporting Information) are not affected by protamine or a mixture of protamine, heparan sulfate, and glutathione. We then tested a second cycle of decondensation and condensation of the decondensed sample. Although the fluorescence intensity of Cy5 was increased (Figure 6F, trace f) and the fluorescence lifetime of QD605 was decreased (Figure 6G, trace f) after the second condensation, evaluation of the degree of DNA condensation was

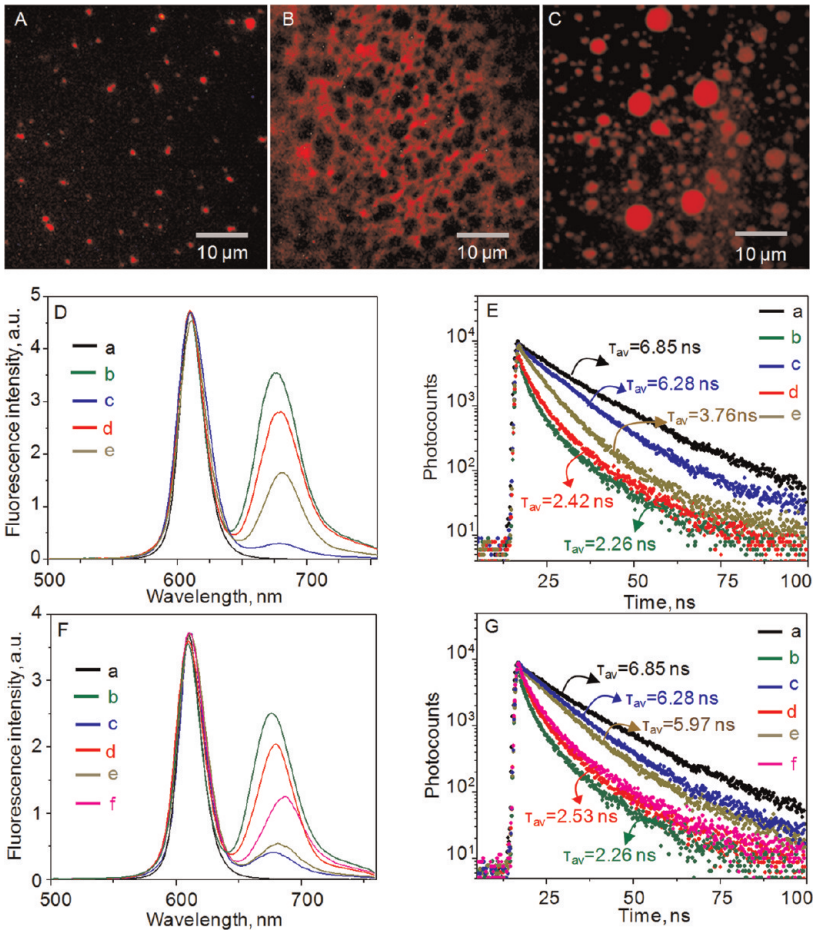

Figure 6. (A–C) Fluorescence images of a solution of pcDNA3.1-GL3 (25 μg/mL) labeled with QD605–Cy5 FRET pair recorded at (A) 5 min, (B) 10 min, and (C) 30 min after treatment with protamine (3 mg/mL). The fluorescence intensity in panel A is graphically enhanced for the clear visualization of the early stage of pDNA condensation. (D,F) Fluorescence spectra and (E,G) nanosecond fluorescence decay profiles of pcDNA labeled using QD605 and Cy5: (a) QD605, (b) as-labeled DNA sample, (c) after FRET-mediated photobleaching of excess Cy5 molecules, (d) after condensation of the photodecomposed sample using protamine (3 mg/mL), (e) after decondensation of the condensed DNA using (D,E) Trisma base (3 mg/mL) or (F,G) a mixture of heparan sulfate and glutathione (3 mg/mL each), and (f) after the addition of excess protamine (6 mg/mL) to the decondensed DNA. The spectra in panels D and F are normalized to the peak of the QD.

technically difficult due to the formation of a white precipitate and scattering of light, which should be due to the formation of a complex between protamine and heparan sulfate.

To analyze the condensation and decondensation processes in pDNA, we estimated the donor-to-acceptor distances at different FRET values by following the methods discussed in refs 83–87 and 89–91. The decondensation of pDNA is more efficient by the heparan sulfate/glutathione mixture than by the Trisma base. Thus, our analysis is focused on the protamine/heparan sulfate–glutathione system. As discussed above, the average fluorescence lifetime of pristine QD605 (6.85 ns) is decreased to 2.26 ns due to the intrinsic FRET from proximal Cy5 molecules; that is, the FRET efficiency before the condensation of pDNA was *ca.* 67%. Because of the intrinsic FRET, the available room for any changes in the FRET value during the condensation of DNA is limited to *ca.* 33%. However, the FRET value was not changed even after the addition of protamine to the DNA sample, indicating that the highest FRET efficiency for the QD605-pDNA-Cy5 system is *ca.* 67%. From the spectral overlap integral and the quantum efficiency of QD605, we estimated the Förster distance of the QD605-Cy5 system at 6.07 nm by following the equations in ref 84. The quantum yield of QDs was estimated at 0.56 using AlexaFluor594 as the standard (Φ = 0.66; Invitrogen). Thus, the FRET value *ca.* 67% in the as-labeled pDNA shows the presence of a Cy5 dye on pDNA within 5.39 nm of QDs, which is not realistic due to the large (≥15 nm) hydrodynamic diameter of the streptavidin conjugated QDs. Thus, multiple Cy5 molecules should be involved in the high FRET efficiency.

To understand the relation between FRET efficiency and the number of Cy5 molecules involved in FRET, we follow the point-dipole approximation proposed for QDs by Medintz and Mattoussi.[90] According to the point-dipole approximation, the Förster formalism of center-to-center distance from a QD to Cy5 is valid in

the estimation of FRET efficiency, just like in the case of organic donor–acceptor systems. Thus, the high FRET efficiency can be interpreted in terms of multiple Cy5 molecules around each QD. We have calculated the approximate distances of the QD to Cy5 molecules on either side in the precondensed pcDNA using the distance between nucleobases in DNA (*ca.* 0.34 nm), the number of base-pairs in pcDNA3.1 (5428), the circumference of pcDNA3.1 (1845.5 nm), the possibility of biotinylation of every nucleobase (protocol in the experimental section), and the DNA:Cy5 (1:150) and DNA:QD (1:15) ratios used in the labeling steps. Thus, the center-to-center distance between adjacent Cy5 molecules should be 12.3 nm and that between adjacent QDs should be 123 nm. In other words, the calculated average distance from the labeling positions in DNA for QD-to-Cy5 (not the center-to-center distance between QD and Cy5) increases on both sides of a QD in the order 6.16, 18.45, 30.75, 43.05, and 55.35 nm up to the limit (61.5 nm) of the neighboring QD. Thus, the FRET efficiencies calculated between one QD and the five Cy5 molecules on either side of the precondensed pcDNA3.1 decrease in the order 47.8%, 0.13%, 5.9×10^{-3}%, 7.9×10^{-4}%, and 1.7×10^{-4}%. However, because of the large hydrodynamic size of the QD, the center-to-center distance between a QD and Cy5 should be larger than the calculated average distance, or, in other words, the FRET efficiency should be much lower than the calculated sum (47.94%). Thus, the experimental intrinsic FRET efficiency (*ca.* 67%) suggests that two or more Cy5 molecules are involved in FRET with each QD, for which one possibility is the presence of multiple Cy5 molecules in the Cy5–streptavidin conjugate. Another possibility is that out of 10 dye molecules placed along the DNA strand at 6.16, 18.45, 30.75, 43.05, and 55.35 nm on either side of a QD, the FRET efficiencies for 6 are negligible ($\ll$0.13%); that is, four Cy5 molecules mainly contribute to the intrinsic FRET (*ca.* 67%). Irrespective of the above two possibilities, the decrease in the intrinsic FRET efficiency from *ca.* 67% to *ca.* 8.3% suggests that nearly 88% of Cy5 molecules proximal to each QD are photobleached by FRET. After the condensation of DNA using protamine, the FRET efficiency is increased from *ca.* 8.8% to *ca.* 61%, indicating that two or more Cy5 molecules kept beyond the limit of FRET-mediated photobleaching fell in close proximity of each QD. The net increase in the FRET efficiency after the condensation (*ca.* 52.2%) suggests that the highest degree of DNA condensation can be from *ca.* 18.45 nm (second Cy5 molecule on either sides of a QD) to the surface of QD. Nevertheless, FRET from QD to Cy5 located at different parts of DNA may have contributions to this value. Also, after the decondensation of the protamine-condensed DNA using heparan sulfate and glutathione, the lifetime of QD is increased from 2.53 to 5.97 ns or the FRET efficiency is lowered to 13% (4.7% after correction for the residual FRET), which suggests that Cy5 molecules move to 10 nm from the center of a QD or beyond.

SUMMARY

We found that FRET-recovery after the photodecomposition (FRET-RAP) of undesired acceptors is an efficient method for the sensitive detection of the condensation and decondensation of pDNA (pcDNA3.1-GL3 and pUC18DNA). The FRET efficiency is first increased by *ca.* 60% during the condensation of pDNA by protamine and successively decreased to *ca.* 5% during the decondensation of the protamine-condensed pDNA using a mixture of heparan sulfate and glutathione. The labeling of pDNA with a small number of highly-photostable energy donors (quantum dots) and a large number of photolabile acceptors followed by the FRET-mediated photodecomposition of acceptors placed within the Förster distance, but without affecting a large number of acceptors placed beyond the Förster distance, is the key to the sensitive detection of the condensation and decondensation steps. Nevertheless, prolonged photoactivation of photosensitizers such as quantum dots for the photodecomposition of undesired acceptors can cause damage to the nucleobases. On the other hand, single-molecule FRET efficiency was negligibly low in the condensed pcDNA3.1-GL3 that was labeled with only one donor and one acceptor through the forward and reverse primers at the upstream and downstream regions of the luciferase GL3 insert present at the multiple cloning sites because of the low probability of the single donor to encounter the single acceptor within the Förster distance. In general, FRET-based photodecomposition of excess acceptors in the proximity of highly photostable donors such as quantum dots will be helpful during the preparation of labeled DNA and other biomolecules for the analyses of not only DNA condensation and gene delivery but also protein–protein and protein–DNA interactions in biophysical investigations.

MATERIALS AND METHODS

We used two plasmid DNA samples: luciferase (GL3)-inserted pcDNA3.1 and pUC18DNA. To prepare the luciferase-encoding vector, an insert fragment encoding luciferase (GL3) was obtained by Hind III/Xba I digestion of the pGL3-basic vector (Promega, USA), and ligated to the *Hin*dIII/Xba I digested site of pcDNA3.1 (Invitrogen, USA).[42] We used two pairs of energy donors and acceptors: QD565–AlexaFluor594 and QD605–Cy5. Streptavidin functionalized QDs (QD565 and QD605) and Ulysis Alexa Fluor594 nucleic acid labeling kit were obtained from

Invitrogen Corporation. Streptavidin functionalized Cy5 and nucleic acid labeling kits for the biotinylation (Label IT-CX-biotin nucleic acid labeling kit) and fluorescence labeling (Label IT Cy5 nucleic acid labeling kit) of DNA were obtained from Mirus Bio Corporation, USA. Biotinylated forward (5′-TTGCGCTGCTTC-GCGATGTACGGGC-3′) and reverse (5′-TAGAATGACACCTACTCA-GACAATG-3′) primers were obtained from Custom DNA Oligos, Sigma-Aldrich Inc. Protamine sulfate salmon mint was obtained from Calbiochem (Darmstadt, Germany). Glutathione, heparan sulfate, and all other reagents and buffers were obtained from Sigma Aldrich, Inc.

Labeling of pcDNA3.1-GL3 and pUC18DNA with Energy Donor−Acceptor Pairs. DNA molecules (pcDNA3.1 and pUC18) were doubly labeled with an energy donor (QD565-streptavidin or QD605-streptavidin) and an energy acceptor (Ulysis Alexa Fluor594 or Cy5-streptavidin). The protocols for the double-labeling of pDNA are outlined in Figure 2. Briefly, the pDNA sample (50 μL, 200 ng/μL) was first dispersed in an optimized buffer supplied with the labeling kit, and then the DNA molecules were denatured at 95 °C for 5 min. The denatured pDNA solutions were mixed with a nucleic acid biotinylation agent (Mirus Label IT-CX-biotin nucleic acid labeling kit, Mirus Corp., USA). This biotinylation agent has the capability to biotinylate every nucleotide. The concentration of the biotinylating agent was set at 1/10th of its concentration in the kit. The mixture was then placed in a 60 °C water bath and incubated at this temperature for 60 min. The biotinylated pDNA was purified by ethanol precipitation and subsequently dispersed in HEPES buffer (pH 7.4) to a concentration of 0.2 mg/mL. The biotinylated pDNA was fractionated into two aliquots. One aliquot was labeled first using Cy5−streptavidin conjugate and then using QD605−streptavidin conjugate. The second aliquot was labeled first using Ulysis Alexa Fluor594 nucleic acid labeling kit and then using QD565−streptavidin conjugate. The labeling of pDNA with QDs, Cy5, and AlexaFluor594 was carried out by following the instructions by the manufacturers. In brief, 10 μL of biotinylated pDNA was suspended in a labeling buffer and reacted with AlexaFluor594 or Cy5−streptavidin under dark at 80 °C for 15 min. The reaction was stopped by snap-cooling. The concentrations of AlexaFluor594 and Cy5−streptavidin were optimized for the introduction of *ca.* 150 dye molecules per pDNA. The dye-labeled pDNA samples were purified using a wizard SV gel and PCR cleanup system (Promega, Inc., USA). This purification was followed by the labeling of the biotin units in pDNA with QD565−streptavidin or QD605−streptavidin at room temperature for 30 min. The concentration of QD−streptavidin conjugates was optimized for the incorporation of *ca.* 15 QDs per pDNA. The QD-labeled pDNA samples were purified using a Sephadex G50 column. The undesired photobleaching of dye molecules was minimized by carrying out all the reactions under minimum room light. Introduction of a large number (1 or more per 18 base pairs) of labels, in particular AlexaFluor594, causes aggregation of DNA. Thus, we set the number of AlexaFluor594 or Cy5 molecules at 1 per 36 base pairs. Yet another potential difficulty in the labeling experiments is the cross-linking between biotin on pDNA and streptavidin on QDs. Although AFM images of QD-labeled pDNA samples in the current work show negligible inter/intramolecular aggregation of DNA or cross-linking of DNA chains, the possibility of aggregation and cross-linking cannot be completely neglected. Also, such aggregation and cross-linking should be carefully considered during the labeling reactions, in particular, when the ratio of biotin and QDs is varied.

The double-labeling of pcDNA3.1 with single-molecule FRET pairs (Cy5-labeled forward primer and QD605-labeled reverse primer) was carried out as follows. First, the forward primer was labeled using Cy5 by the incubation of the biotinylated primer with Cy5−streptavidin conjugate at 1:1 molar equivalence for 30 min at room temperature. Similarly, the reverse primer was labeled using QD605−streptavidin conjugate. Next, the labeled primers were purified by desalting and subsequently incorporated into the pcDNA3.1 as shown in Figure 2B. The pcDNA sample was first dispersed in an optimized buffer supplied with it, and then denatured at 95 °C for 20 min. Finally, the denatured pcDNA was treated with a mixture (1:1) of Cy5-conjugated forward primer and QD605-conjugated reverse primer, and annealed for 10 min by placing the sample in a water bath kept at 65 °C. During this annealing, the labeled primers bind at the primer binding sites in pcDNA3.1. The primer-labeled pcDNA3.1 sample was purified using the wizard SV gel and PCR cleanup system.

Atomic Force Microscopy (AFM) Imaging. Tapping-mode AFM images of the donor- and acceptor-labeled pDNA samples were collected in air using a MFP-3D microscope (Asylum Research, Santa Barbara, USA). The microscope was equipped with reflective aluminum-coated ultrasharp (radius of curvature ~10 nm) silicon nanoprobes (Olympus, Japan). The cantilevers used were 160 μm long, and had a spring constant of 42 N/m and a resonance frequency of ~300 kHz.

Fluorescence Imaging and Time-Resolved Fluorescence Measurements. Fluorescence images of pDNA before and after the condensation using protamine were recorded in an inverted optical microscope (Olympus IX 71) that was equipped with a 60× objective lens (Olympus, NA 0.98). Fluorescence signal collected using the objective lens was filtered through band-pass or long-pass filters for QD565, QD605, Alexa Fluor594, or Cy5, magnified using a 2.5× telescopic lens, and recorded using an image intensifier/charge-coupled device assembly (Hamamatsu Photonics).

Nanosecond fluorescence decay profiles and time-resolved fluorescence spectra of the doubly labeled pDNA were recorded using an assembly of a polychromator (Chromex-250IS) and a photon-counting streak-camera (Hamamatsu-C4334). The donors in the doubly labeled pDNA samples were selectively excited using 400 nm pulses (150 fs) generated from the SHG crystal of an optical parametric amplifier (Coherent OPA 9400). The OPA was pumped at 200 kHz by a regenerative amplifier (Coherent RegA 9000) that was seeded by a mode-locked Ti:sapphire laser (Coherent Mira 900F). The fluorescence signals from QDs, AlexaFluor594, and Cy5 were collected through suitable band-pass or long-pass filters and focused at the entrance slit of the polychromator.

Evaluation of FRET Efficiency. The efficiency of energy transfer in a FRET system is given by $E = 1/[1 + (r/R_0)^6]$, where r is the distance between the donor and acceptor and R_0 is the Förster distance of the donor−acceptor pair, that is, the distance at which the efficiency of energy transfer is 50%. The value of R_0 is given by $R_0 = [9\Phi_0(\ln 10)\kappa^2\ J]/(128\pi^5 n^4 N_A)$, where Φ_0 is the fluorescence quantum efficiency of the donor, κ^2 is the donor-to-acceptor dipole orientation factor, J is the spectral overlap integral, n is the refractive index of the medium and N_A is Avogadro's number. The spectral overlap integral is given by $J = \int f_D(\lambda)\epsilon_A(\lambda)\lambda^4\, d\lambda$; where f_D is the normalized emission spectrum of the donor, λ is wavelength, and ϵ_A is the molar extinction coefficient of the acceptor. Because experimental estimation of all the above parameters is tedious, FRET efficiency is evaluated more directly using $E = 1 - (\Phi_{D\text{-}A}/\Phi_D)$ or $E = 1 - (\tau_{D\text{-}A}/\tau_D)$, where $\Phi_{D\text{-}A}$ and $\tau_{D\text{-}A}$ are respectively the fluorescence quantum efficiency and lifetime of donor in the FRET pair system, and Φ_D and τ_D are respectively the fluorescence quantum efficiency and lifetime of pristine donor. We calculated the FRET efficiency using the average fluorescence lifetimes of QDs. The average lifetime values are estimated as $\tau_{av} = (\tau_1\alpha_1 + \tau_2\alpha_2 + \tau_3\alpha_3)/(\alpha_1 + \alpha_2 + \alpha_3)$; where, τ_1, τ_2, and τ_3 are the individual lifetime values, and α_1, α_2, and α_3 are the corresponding amplitudes.

Conflict of Interest: The authors declare no competing financial interest.

Acknowledgment. This work is supported by a special coordination fund for Promoting Science and Technology of the Ministry of Education, Culture, Sports, Science and Technology (MEXT) of the Japanese Government. Also, this work is supported (to V.B.) by Precursory Research for Embryonic Science and Technology (PRESTO), the Japan Science and Technology Agency.

Supporting Information Available: Temporal changes in the nanosecond fluorescence decay profiles and fluorescence spectra of pcDNA3.1-GL3 labeled using QD565/AlexaFluor594 or QD605/Cy5 FRET pairs, fluorescence decay profiles, and

fluorescence spectra of QD565 and QD605 as a function of time under photoactivation at 400 nm, fluorescence decay profiles and fluorescence spectra of QD565 and QD605 in the presence and absence of protamine or a mixture of heparan sulfate and glutathione, AFM images of pDNA labeled with excess Alexa-Fluor594 or QDs, and fluorescence spectra and decay profiles of QD565 and QD605-labeled pDNA in the presence and absence of protamine. This material is available free of charge *via* the Internet at http://pubs.acs.org.

REFERENCES AND NOTES

1. Mulligan, R. C. The Basic Science of Gene-Therapy. *Science* **1993**, *260*, 926–932.
2. Boussif, O.; Lezoualch, F.; Zanta, M. A.; Mergny, M. D.; Scherman, D.; Demeneix, B.; Behr, J. P. A Versatile Vector for Gene and Oligonucleotide Transfer into Cells in Culture and *in-Vivo* Polyethylenimine. *Proc. Natl. Acad. Sci. U.S.A.* **1995**, *92*, 7297–7301.
3. Naldini, L.; Blomer, U.; Gallay, P.; Ory, D.; Mulligan, R.; Gage, F. H.; Verma, I. M.; Trono, D. *In Vivo* Gene Delivery and Stable Transduction of Nondividing Cells by a Lentiviral Vector. *Science* **1996**, *272*, 263–267.
4. Kataoka, K.; Harada., A.; Nagasaki, Y. Block Copolymer Micelles for Drug Delivery: Design, Characterization and Biological Significance. *Adv. Drug Delivery Rev.* **2001**, *47*, 113–131.
5. Torchilin, V. P. Recent Advances with Liposomes as Pharmaceutical Carriers. *Nat. Rev. Drug. Discovery* **2005**, *4*, 145–160.
6. Abeylath, S. C.; Ganta, S.; Iyer, A. K.; Amiji, M. Combinatorial-Designed Multifunctional Polymeric Nanosystems for Tumor-Targeted Therapeutic Delivery. *Acc. Chem. Res.* **2011**, *44*, 1009–1017.
7. Malakoutikhah, M.; Teixidóo, M.; Giralt, E. Shuttle-Mediated Drug Delivery to the Brain. *Angew. Chem., Int. Ed.* **2011**, *50*, 7998–8014.
8. Huang, Y. H.; Fang, C. C.; Tsuneyama, K.; Chou, H. Y.; Pan, W. Y.; Shih, Y. M.; Wu, P. Y.; Chen, Y.; Leung, P. S. C.; Gershwin, M. E.; *et al.* A Murine Model of Hepatitis B-Associated Hepatocellular Carcinoma Generated by Adeno-Associated Virus-Mediated Gene Delivery. *Int. J. Oncol.* **2011**, *39*, 1511–1519.
9. Kane, M.; Case, K. L.; Kopaskie, K.; Kozlova, A.; MacDearmid, C.; Chervonsky, A. V.; Golovkina, T. V. Successful Transmission of a Retrovirus Depends on the Commensal Microbiota. *Science* **2011**, *334*, 245–249.
10. Mintzer, M. A.; Simanek, E. E. Nonviral Vectors for Gene Delivery. *Chem. Rev.* **2009**, *109*, 259–302.
11. Lim, K. I.; Klimczak, R.; Yu, J. H.; Schaffer, D. V. Specific Insertions of Zinc Finger Domains into Gag-Pol Yield Engineered Retroviral Vectors with Selective Integration Properties. *Proc. Natl. Acad. Sci. U.S.A.* **2010**, *109*, 12475–12480.
12. Kay, M. A.; Glorioso, J. C.; Naldini, L. Viral Vectors for Gene Therapy: The Art of Turning Infectious Agents into Vehicles of Therapeutics. *Nat. Med.* **2001**, *7*, 33–40.
13. Letvin, N. L.; Montefiori, D. C.; Yasutomi, Y.; Perry, H. C.; Davies, M. E.; Lekutis, C.; Alroy, M.; Freed, D. C.; Lord, C. I.; Handt, L. K.; *et al.* Potent, Protective Anti-HIV Immune Responses Generated by Bimodal HIV Envelope DNA Pins Protein Vaccination. *Proc. Natl. Acad. Sci. U.S.A.* **1997**, *94*, 9378–9383.
14. Letvin, N. L. Progress in the Development of an HIV-1 Vaccine. *Science* **1998**, *280*, 1875–1880.
15. Hoffmann, E.; Krauss, S.; Perez, D.; Webby, R.; Webster, R. G. Eight-Plasmid System for Rapid Generation of Influenza Virus Vaccines. *Vaccine* **2002**, *20*, 3165–3170.
16. Wei, C. J.; Boyington, J. C.; McTamney, P. M.; Kong, W. P.; Pearce, M. B.; Xu, L.; Andersen, H.; Rao, S.; Tumpey, T. M.; Yang, Z. Y.; *et al.* Induction of Broadly Neutralizing H1N1 Influenza Antibodies by Vaccination. *Science* **2010**, *329*, 1060–1064.
17. Adelman, Z. N.; Sanchez-Vargas, I.; Travanty, E. A.; Carlson, J. O.; Beaty, B. J.; Blair, C. D.; Olson, K. E. RNA Silencing of Dengue Virus Type 2 Replication in Transformed C6/36 Mosquito Cells Transcribing an Inverted-Repeat RNA Derived from the Virus Genome. *J. Virol.* **2002**, *76*, 12925–12933.
18. Garcia-Hernandez, E.; Gonzalez-Sanchez, J. L.; Andrade-Manzano, A.; Contreras, M. L.; Padilla, S.; Guzman, C. C.; Jimenez, R.; Reyes, L.; Morosoli, G.; Kerde, M. L.; *et al.* Regression of Papilloma High-Grade Lesions (CIN 2 and CIN 3) Is Stimulated by Therapeutic Vaccination with MVA E2 Recombinant Vaccine. *Cancer Gene Ther.* **2006**, *13*, 592–597.
19. Davis, H. L.; McCluskie, M. J.; Gerin, J. L.; Purcell, R. H. DNA Vaccine for Hepatitis B: Evidence for Immunogenicity in Chimpanzees and Comparison with Other Vaccines. *Proc. Natl. Acad. Sci. U.S.A.* **1996**, *93*, 7213–7218.
20. Arold, S. T.; Leonard, P. G.; Parkinson, G. N.; Ladbury, J. E. H-NS Forms a Superhelical Protein Scaffold for DNA Condensation. *Proc. Natl. Acad. Sci. U.S.A.* **2010**, *107*, 15728–15732.
21. Samson, J.; Varotto, A.; Nahirney, P. C.; Toschi, A.; Piscopo, I.; Drain, C. M. Fabrication of Metal Nanoparticles Using Toroidal Plasmid DNA as a Sacrificial Mold. *ACS Nano* **2009**, *3*, 339–344.
22. Ghosh, P. S.; Kim, C. K.; Han, G.; Forbes, N. S.; Rotello, V. M. Efficient Gene Delivery Vectors by Tuning the Surface Charge Density of Amino Acid-Functionalized Gold Nanoparticles. *ACS Nano* **2008**, *2*, 2213–2218.
23. Khaled, A.; Guo, S. C.; Li, F.; Guo, P. X. Controllable Self-Assembly of Nanoparticles for Specific Delivery of Multiple Therapeutic Molecules to Cancer Cells Using RNA Nanotechnology. *Nano Lett.* **2005**, *5*, 1797–1808.
24. Pantarotto, D.; Singh, R.; McCarthy, D.; Erhardt, M.; Briand, J. P.; Prato, M.; Kostarelos, K.; Bianco, A. Functionalized Carbon Nanotubes for Plasmid DNA Gene Delivery. *Angew. Chem., Int. Ed.* **2004**, *43*, 5242–5246.
25. Singh, R.; Pantarotto, D.; McCarthy, D.; Chaloin, O.; Hoebeke, J.; Partidos, C. D.; Briand, J. P.; Prato, M.; Bianco, A.; Kostarelos, K. Binding and Condensation of Plasmid DNA onto Functionalized Carbon Nanotubes: Toward the Construction of Nanotube-Based Gene Delivery Vectors. *J. Am. Chem. Soc.* **2005**, *127*, 4388–4396.
26. Kam, N. W. S.; Liu, Z.; Dai, H. J. Functionalization of Carbon Nanotubes *via* Cleavable Disulfide Bonds for Efficient Intracellular Delivery of siRNA and Potent Gene Silencing. *J. Am. Chem. Soc.* **2005**, *127*, 12492–12493.
27. Wagner, E.; cotton, M.; Foisner, R.; Birnstiel, M. L. Transferrin Polycation DNA Complexes —The Effect of Polycations on the Structure of the Complex and DNA Delivery to Cells. *Proc. Natl. Acad. Sci. U.S.A.* **1991**, *88*, 4255–4259.
28. Bloomfield, V. A. DNA Condensation by Multivalent Cations. *Biopolymers* **1997**, *44*, 269–282.
29. Thomas, M.; Klibanov, A. M. Non-viral Gene Therapy: Polycation-Mediated DNA Delivery. *Appl. Miocrobiol. Biotechnol.* **2003**, *62*, 27–34.
30. Melnikov, S. M.; Sergeyev, V. G.; Yoshikawa, K. Transition of Double-Stranded DNA Chains between Random Coil and Compact Globule States Induced by Cooperative Binding of Cationic Surfactant. *J. Am. Chem. Soc.* **1995**, *117*, 9951–9956.
31. Melnikov, S. M.; Sergeyev, V. G.; Yoshikawa, K. Discrete Coil-Globule Transition of Large DNA Induced by Cationic Surfactant. *J. Am. Chem. Soc.* **1995**, *117*, 2401–2408.
32. Saccardo, P.; Villaverde, A.; Gonzalez-Montalban, N. Peptide-Mediated DNA Condensation for Non-viral Gene Therapy. *Biotechnol. Adv.* **2009**, *27*, 432–438.
33. Vazquez, M. E.; Caamano, A. M.; Mascarenas, J. L. From Transcription Factors to Designed Sequence-Specific DNA-Binding Peptides. *Chem. Soc. Rev.* **2003**, *32*, 338–349.
34. Sasaki, N.; Kuroiwa, H.; Nishitani, C.; Takano, H.; Higashiyama, T.; Kobayashi, T.; Shirai, Y.; Sakai, A.; Kawano, S.; Murakami-Murofushi, K.; *et al.* Glom is a Novel Mitochondrial DNA Packaging Protein in *Physarum Polycephalum* and Causes Intense Chromatin Condensation without Suppressing DNA Functions. *Mol. Biol. Cell* **2003**, *14*, 4758–4769.

35. Felgner, P. L.; Gadek, T. R.; Holm, M.; Roman, R.; Chan, H. W.; Wenz, M.; Northrop, J. P.; Ringold, G. M.; Danielsen, M. Lipofection—A Highly Efficient, Lipid-Mediated DNA-Transfection Procedure. *Proc. Natl. Acad. Sci. U.S.A.* **1987**, *84*, 7413–7417.
36. Matulis, D.; Rouzina, I.; Bloomfield, V. A. Thermodynamics of Cationic Lipid Binding to DNA and DNA Condensation: Roles of Electrostatics and Hydrophobicity. *J. Am. Chem. Soc.* **2002**, *124*, 7331–7342.
37. Wurpel, G. W. H.; Sovago, M.; Bonn, M. Sensitive Probing of DNA Binding to a Cationic Lipid Monolayer. *J. Am. Chem. Soc.* **2007**, *129*, 8420–8421.
38. Jones, J. J.; van der Maarel, J. R. C.; Doyle, P. S. Effect of Nanochannel Geometry on DNA Structure in the Presence of Macromolecular Crowding Agent. *Nano Lett.* **2011**, *11*, 5047–5053.
39. Zhang, C.; Shao, P. G.; van Kan, J. A.; van der Maarel, J. R. C. Macromolecular Crowding Induced Elongation and Compaction of Single DNA Molecules Confined in a Nanochannel. *Proc. Natl. Acad. Sci. U.S.A.* **2009**, *106*, 16651–16656.
40. Li, G.-W.; Berg, O. G.; Elf, J. Effects of Macromolecular Crowding and DNA Looping on Gene Regulation Kinetics. *Nat. Phys.* **2009**, *5*, 294–297.
41. De Smedt, S. C.; Remaut, K.; Lucas, B.; Braeckmans, K.; Sanders, N. N.; Demeester, J. Studying Biophysical Barriers to DNA Delivery by Advanced Light Microscopy. *Adv. Drug Delivery Rev.* **2005**, *57*, 191–210.
42. Shaheen, S. M.; Akita, H.; Yamashita, A.; Katoono, R.; Yui, N.; Biju, V.; Ishikawa, M.; Harashima, H. Quantitative Analysis of Condensation/Decondensation Status of pDNA in the Nuclear Sub-domains by QD-FRET. *Nucleic Acids Res.* **2011**, *39*, e48.
43. Raty, J. K.; Liimatainen, T.; Kaikkonen, M. U.; Grahn, O.; Airenne, K. J.; Yla-Herttuala, S. Non-invasive Imaging in Gene Therapy. *Mol. Ther.* **2007**, *15*, 1579–1586.
44. Wang, P.; Zhao, X.-H.; Wang, Z.-Y.; Meng, M.; Li, X.; Ning, Q. Generation 4 Polyamidoamine Dendrimers is a Novel Candidate of Nanocarrier for Gene Delivery Agents in Breast Cancer Treatment. *Cancer Lett.* **2010**, *298*, 34–49.
45. Gosule, L. C.; Schellman, J. A. Compact Form of DNA Induced by Spermidine. *Nature* **1976**, *259*, 333–335.
46. Marx, K. A.; Reynolds, T. C. Spermidine-Condensed φX174 DNA Cleavage by Micrococcal Nuclease: Torus Cleavage Model and Evidence for Unidirectional Circumferential DNA Wrapping. *Proc. Natl. Acad. Sci. U.S.A.* **1982**, *79*, 6484–6488.
47. Eickbush, T. H.; Moudrianakis, E. N. The Compaction of DNA Helices into either Continuous Supercoils or Folded-Fiber Rods and Toroids. *Cell* **1978**, *13*, 295–306.
48. Wilson, R. W.; Bloomfield, V. A. Counterion-Induced Condensation of Deoxyribonucleic Acid. A Light-Scattering Study. *Biochemistry* **1979**, *18*, 2192–2196.
49. Vijayanathan, V.; Thomas, T.; Antony, T.; Shirahata, A.; Thomas, T. J. Formation of DNA Nanoparticles in the Presence of Novel Polyamine Analogues: A Laser Light Scattering and Atomic Force Microscopic Study. *Nucleic Acids Res.* **2004**, *32*, 127–134.
50. Dunlap, D. D.; Maggi, A.; Soria, M. R.; Monaco, L. Nanoscopic Structure of DNA Condensed for Gene Delivery. *Nucleic Acids Res.* **1997**, *25*, 3095–3101.
51. Fang, Y.; Hoh, J. H. Early Intermediates in Spermidine Induced Condensation on the Surface of Mica. *J. Am. Chem. Soc.* **1998**, *120*, 8903–8909.
52. Böttcher, C.; Endisch, C.; Fuhrhop, J. H.; Catterall, C.; Eaton, M. High Yield Preparation of Oligomeric C-Type DNA Toroids and Their Characterization by Cryoelectron Microscopy. *J. Am. Chem. Soc.* **1998**, *120*, 12–17.
53. Simberg, D.; Danino, D.; Talmon, Y.; Minsky, A.; Ferrari, M. E.; Wheeler, C. J.; Barenholz, Y. Phase Behavior, DNA Ordering, and Size Instability of Cationic Lipoplexes—Relevance to Optimal Transfection Activity. *J. Biol. Chem.* **2001**, *276*, 47453–47459.
54. Cui, L.; Chen, D.; Zhu, L. Conformation Transformation Determined by Different Self-Assembled Phases in a DNA Complex with Cationic Polyhedral Oligomeric Silsesquioxane Lipid. *ACS Nano* **2008**, *2*, 921–927.
55. Bello-Roufai, M.; Lambert, O.; Pitard, B. Relationships between the Physicochemical Properties of an Amphiphilic Triblock Copolymers/DNA Complexes and Their Intramuscular Transfection Efficiency. *Nucleic Acids Res.* **2007**, *35*, 728–739.
56. Stein, I. H.; Steinhauer, C.; Tinnefeld, P. Single-Molecule Four-Color FRET Visualizes Energy-Transfer Paths on DNA Origami. *J. Am. Chem. Soc.* **2011**, *133*, 4193–4195.
57. Sabir, T.; Schroder, G. F.; Toulmin, A.; McGlynn, P.; Magennis, S. W. Global Structure of Forked DNA in Solution Revealed by High-Resolution Single-Molecule FRET. *J. Am. Chem. Soc.* **2011**, *133*, 1188–1191.
58. Jiang, G. X.; Susha, A. S.; Lutich, A. A.; Stefani, F. D.; Feldmann, J.; Rogach, A. L. Cascaded FRET in Conjugated Polymer/Quantum Dot/Dye-Labeled DNA Complexes for DNA Hybridization Detection. *ACS Nano* **2009**, *3*, 4127–4131.
59. Ho, Y. P.; Chen, H. H.; Leong, K. W.; Wang, T. H. Evaluating the Intracellular Stability and Unpacking of DNA Nanocomplexes by Quantum Dots-FRET. *J. Controlled Release* **2006**, *116*, 83–89.
60. Breuzard, G.; Tertil, M.; Goncalves, C.; Cheradame, H.; Geguan, P.; Pichon, C.; Midoux, P. Nuclear Delivery of N Kappa B-Assisted DNA/Polymer Complexes: Plasmid DNA Quantitation by Confocal Laser Scanning Microscopy and Evidence of Nuclear Polyplexes by FRET Imaging. *Nucleic Acids Res.* **2008**, *36*, e71.
61. Peng, H.; Zhang, L. J.; Kjallman, T. H. M.; Soeller, C.; Travas-Sejdic, J. DNA Hybridization Detection with Blue Luminescent Quantum Dots and Dye-Labeled Single-Stranded DNA. *J. Am. Chem. Soc.* **2007**, *129*, 3048–3049.
62. Sacca, B.; Meyer, R.; Niemeyer, C. M. Temperature-Dependent FRET Spectroscopy for The High-Throughput Analysis of Self-Assembled DNA Nanostructures in Real Time. *Nat. Protoc.* **2009**, *4*, 271–285.
63. Woźniak, A. C.; Schröder, G. F.; Grubmüller, H.; Seidel, C. A. M.; Oesterhelt, F. Single-Molecule FRET Measures Bends and Kinks in DNA. *Proc. Natl. Acad. Sci. U.S.A.* **2008**, *105*, 18337–18342.
64. Sacca, B.; Meyer, R.; Feldkamp, U.; Schroeder, H.; Niemeyer, C. M. High-Throughput, Real-Time Monitoring of the Self-Assembly of DNA Nanostructures by FRET Spectroscopy. *Angew. Chem., Int. Ed.* **2008**, *47*, 2135–2137.
65. Muller, B. K.; Reuter, A.; Simmel, F. C.; Lamb, D. C. Single-Pair FRET Characterization of DNA Tweezers. *Nano Lett.* **2006**, *6*, 2814–2820.
66. Suzuki, M.; Husimi, Y.; Komatsu, H.; Suzuki, K.; Douglas, K. T. Quantum Dot FRET Biosensors that Respond to pH, to Proteolytic or Nucleolytic Cleavage, to DNA Synthesis, or to a Multiplexing Combination. *J. Am. Chem. Soc.* **2008**, *130*, 5720–5725.
67. Radman-Livaja, M.; Biswas, T.; Mierke, D.; Landy, A. Architecture of Recombination Intermediates Visualized by In-Gel FRET of Lambda Integrase-Holliday Junction-Arm DNA Complexes. *Proc. Natl. Acad. Sci. U.S.A.* **2005**, *102*, 3913–3920.
68. Lakowicz, J. R. *Principles of Fluorescence Spectroscopy*, 2nd ed.; 1999; Kluwer/Plenum, New York.
69. Sapsford, K. E.; Berti, L.; Medintz, I. L. Materials for Fluorescence Resonance Energy Transfer Analysis: Beyond Traditional Donor−Acceptor Combinations. *Angew. Chem., Int. Ed.* **2006**, *45*, 4562–4589.
70. Chen, H. H.; Ho, Y. P.; Jiang, X.; Mao, H. Q.; Wang, T. H.; Leong, K. W. Simultaneous Non-invasive Analysis of DNA Condensation and Stability by Two-Step QD-FRET. *Nano Today* **2009**, *4*, 125–134.
71. Wang, S.; Gaylord, B. S.; Bazan, G. C. Fluorescein Provides a Resonance Gate for FRET from Conjugated Polymers to DNA Intercalated Dyes. *J. Am. Chem. Soc.* **2004**, *126*, 5446–5451.
72. Walsh, A. S.; Yin, H.; Erben, C. M.; Wood, M. J. A.; Turberfield, A. J. DNA Cage Delivery to Mammalian Cells. *ACS Nano* **2011**, *7*, 5427–5432.
73. Choi, J.; Kim, S.; Tachikawa, T.; Fujitsuka, M.; Majima, T. pH-Induced Intramolecular Folding Dynamics of i-Motif DNA. *J. Am. Chem. Soc.* **2011**, *133*, 16146–16153.
74. Simmons, C. R.; Schmitt, D.; Wei, X.; Han, D.; Volosin, A. M.; Ladd, D. M.; Seo, D.-K.; Liu, Y.; Yan, H. Size-Selective

Incorporation of DNA Nanocages into Nanoporous Antimony-Doped Tin Oxide Materials. *ACS Nano* **2011**, *5*, 6060–6068.
75. Zhang, B.; Zhang, Y.; Mallapragada, S. K.; Clapp, A. R. Sensing Polymer/DNA Polyplex Dissociation Using Quantum Dot Fluorophores. *ACS Nano* **2011**, *5*, 129–138.
76. Boeneman, K.; Deschamps, J. R.; Buckhout-White, S.; Prasuhn, D. E.; Blanco-Canosa, J. B.; Dawson, P. E.; Stewart, M. H.; Susumu, K.; Goldman, E. R.; Ancona, M.; *et al*. Quantum Dot DNA Bioconjugates: Attachment Chemistry Strongly Influences the Resulting Composite Architecture. *ACS Nano* **2010**, *4*, 7253–7266.
77. Ray, R.; Ma, J.; Oram, M.; Lakowicz, J. R.; Black, L. W. Single-Molecule and FRET Fluorescence Correlation Spectroscopy Analyses of Phage DNA Packaging: Colocalization of Packaged Phage T4 DNA Ends within the Capsid. *J. Mol. Biol.* **2010**, *395*, 1102–1113.
78. Medintz, I. L.; Clapp, A. R.; Mattoussi, H.; Goldman, E. R.; Fisher, B.; Mauro, J. M. Self-Assembled Nanoscale Biosensors Based on Quantum Dot FRET Donors. *Nat. Mater.* **2003**, *2*, 630–638.
79. Biju, V.; Itoh, T.; Ishikawa, M. Delivering Quantum Dots to Cells: Bioconjugated Quantum Dots for Targeted and Nonspecific Extracellular and Intracellular Imaging. *Chem. Soc. Rev.* **2010**, *39*, 3031–3056.
80. Biju, V.; Itoh, T.; Anas, A.; Sujith, A.; Ishikawa, M. Semiconductor Quantum Dots and Metal Nanoparticles: Syntheses, Optical Properties, and Biological Applications. *Anal. Bioanal. Chem.* **2008**, *391*, 2469–2495.
81. Anas, A.; Okuda, T.; Kawashima, N.; Nakayama, K.; Itoh, T.; Ishikawa, M. Clathrin-Mediated Endocytosis of Quantum Dot−Peptide Conjugates in Living Cells. *ACS Nano* **2009**, *3*, 2419–2429.
82. Biju, V.; Mundayoor, S.; Omkumar, R. V.; Anas, A.; Ishikawa, M. Bioconjugated Quantum Dots for Cancer Research: Present Status, Prospects and Remaining Issues. *Biotechnol. Adv.* **2010**, *28*, 199–213.
83. Willard, D. M.; Carillo, L. L.; Jung, J.; Orden, A. V. CdSe−ZnS Quantum Dots as Resonance Energy Transfer Donors in a Model Protein−Protein Binding Assay. *Nano Lett.* **2001**, *1*, 469–474.
84. Clapp, A. R.; Medintz, I. L.; Mauro, J. M.; Fisher, B. R.; Bawendi, M. G.; Mattoussi, H. Fluorescence Resonance Energy Transfer Between Quantum Dot Donors and Dye-Labeled Protein Acceptors. *J. Am. Chem. Soc.* **2004**, *126*, 301–310.
85. Goldman, E. R.; Medintz, I. L.; Whitley, J. L.; Hayhurst, A.; Clapp, A, R.; Uyeda, T.; Deschamps, J. R.; Lassman, M. E.; Mattoussi, H. A Hybrid Quantum Dot-Antibody Fragment Fluorescence Resonance Energy Transfer-Based TNT Sensor. *J. Am. Chem. Soc.* **2005**, *127*, 6744–6751.
86. Zhang, C. Y.; Yen, H. C.; Kuroki, M. T.; Wang, T. H. Single-Quantum-Dot-Based DNA Nanosensors. *Nat. Mater.* **2005**, *4*, 826–829.
87. Bagalkot, V.; Zhang, L.; Nissenbaum, E. L.; Jon, S.; Kantoff, P. W.; Langer, R.; Omid, C.; Farokhzad, O. C. Quantum Dot−Aptamer Conjugates for Synchronous Cancer Imaging, Therapy, and Sensing of Drug Delivery Based on Bi-fluorescence Resonance Energy Transfer. *Nano Lett.* **2007**, *7*, 3065–3070.
88. Anas, A.; Akita, H.; Harashima, H.; Itoh, T.; Ishikawa, M.; Biju, V. Photosensitized Breakage and Damage of DNA by CdSe−ZnS Quantum Dots. *J. Phys. Chem. B* **2008**, *112*, 10005–10011.
89. Rogach, A. L. Fluorescence Energy Transfer in Hybrid Structures of Semiconductor Nanocrystals. *Nano Today* **2011**, *6*, 355–365.
90. Medintz, I. L.; Mattoussi, H. Quantum Dot-Based Resonance Energy Transfer and Its Growing Application in Biology. *Phys. Chem. Chem. Phys.* **2009**, *11*, 17–45.
91. Algar, W. R.; Tavares, A. J.; Krull, U. J. Beyond Labels: A Review of the Application of Quantum Dots as Integrated Components of Assays, Bioprobes, and Biosensors Utilizing Optical Transduction. *Anal. Chim. Acta* **2010**, *673*, 1–25.